

**Nanowire lasers as intracellular probes**

Journal:	<i>Nanoscale</i>
Manuscript ID	NR-ART-01-2018-000515.R1
Article Type:	Paper
Date Submitted by the Author:	16-Apr-2018
Complete List of Authors:	Wu, Xiaoqin; University of Michigan, Biomedical Engineering Chen, Qiushu; University of Michigan, Biomedical Engineering Xu, Peizhen; Zhejiang University Chen, Yu-Cheng; University of Michigan, Biomedical Engineering Wu, Bimin; University of Michigan, Biomedical Engineering Coleman, Rhima; University of Michigan, Biomedical Engineering Tong, Limin; Zhejiang University, Department of Optical Engineering Fan, Xudong; University of Michigan, Biomedical Engineering

Nanowire lasers as intracellular probes

Xiaoqin Wu,^{1,2} Qiushu Chen,¹ Peizhen Xu,² Yu-Cheng Chen,¹ Biming Wu,¹ Rhima M. Coleman,^{1,3} Limin Tong,² and Xudong Fan^{1,a)}

¹Department of Biomedical Engineering, University of Michigan, 1101 Beal Avenue, Ann Arbor, Michigan 48109, USA

²State Key Laboratory of Modern Optical Instrumentation, College of Optical Science and Engineering, Zhejiang University, Hangzhou 310027, China

³Department of Mechanical Engineering, University of Michigan, 1101 Beal Avenue, Ann Arbor, Michigan 48109, USA

Abstract

We investigate a cadmium sulfide (CdS) nanowire (NW) laser that is spontaneously internalized into a single cell to serve as a stand-alone intracellular probe. By pumping with nano-joule light pulses, green laser emission (500-520 nm) can be observed inside cells with a peak linewidth as narrow as 0.5 nm. Due to the sub-micron diameter (~200 nm), the NW has an appreciable fraction of the evanescent field outside, facilitating a sensitive detection of the cellular environmental changes. By monitoring the lasing peak wavelength shift in response to the intracellular refractive index change, our NW laser probe shows a sensitivity of 55 nm/RIU (refractive index units) and a figure of merit of approximately 98.

Introduction

Biological probes based on pillars,¹⁻³ wires,⁴⁻⁹ particles,¹⁰⁻¹³ beads,¹⁴⁻¹⁷ and tubes,¹⁸⁻²¹ which can safely pass through the plasma membrane and enter a living cell, have found wide applications in gene and drug delivery, bio-sensing, electrochemistry, and electrophysiology. Among them, optical bio-probes such as dyes, fluorescent proteins, quantum dots, and plasmonic nanoparticles play an important role in understanding cell biology and in biomedical engineering.¹⁰⁻¹² However, those fluorescent and luminescent probes usually have broad emission spectra (i.e., 30-100 nm), which, to a certain degree, limit their applications in spectral multiplexing,¹⁵ high-resolution imaging,²² and ultra-sensitive bio-sensing.²³ To address this issue, intracellular laser probes, with the advantage of narrow linewidth, strong coherence, and threshold-gated nonlinear emission were proposed.^{14,15,17} Based on microsphere structures, which serve as whispering gallery mode resonators, several intracellular dielectric lasers have been reported using doped fluorescent dyes as the gain media, including injected oil droplets, natural lipid droplets, and polystyrene microbeads.^{14,15,17} Such lasers have extremely narrow linewidths (limited by the spectrometer resolution) and relatively low lasing thresholds of a few $\mu\text{J}/\text{mm}^2$ per pulse. However, the smallest intracellular dielectric laser demonstrated so far utilizes a dye-mixed polyphenyl ether sphere droplet of 7 μm in diameter,¹⁴ corresponding to a volume of 180 μm^3 , which is relatively large for a cell to intake and limit the number of the probes that one cell can internalize. Recently, plasmon-based nanosphere lasers (spasers) with a diameter of 22 nm were reported to generate laser emission directly inside living cells.¹³ However, their lasing threshold is high ($\sim 260 \mu\text{J}/\text{mm}^2$), close to the laser exposure limit for tissues ($\sim 200 \mu\text{J}/\text{mm}^2$).²⁴ Significant reduction of the lasing probe volume while maintaining a cell-amicable lasing threshold is highly desired to minimize invasive perturbations to and increase the number of probes inside a cell.

Semiconductor NWs, with sub-micron diameters and lengths of only a few micrometers, can simultaneously act the optical cavity and possess the gain medium, making them an excellent candidate for stand-alone laser probes.^{22,25-27} In addition, owing to their appreciable fraction of the electric field outside the surface, NWs show strong evanescent interaction with the surrounding medium, which can be exploited for sensitive detection of intracellular environment changes (e.g., RI change) near the NWs.²⁸ In this work, we introduce cadmium sulfide (CdS) NW lasers as intracellular probes (Fig. 1a). The size of the lasing NWs is chosen to have the

diameter ranging from 190 nm to 250 nm and the length ranging from 3.5 μm to 7 μm , corresponding to a volume of 0.1 μm^3 -0.34 μm^3 , which is over three orders of magnitudes smaller than the previously reported microsphere-based lasers.^{14,15,17} The threshold of these NWs is a few $\mu\text{J}/\text{mm}^2$, about one or two orders of magnitudes lower than that for the spaser probes.¹³ By detecting the lasing wavelength shift in response to the intracellular environment changes, our NW lasing probe shows a sensitivity of 55 nm/RIU (refractive index units) and a figure of merit (FOM) of approximately 98.

Experimental

The CdS NWs are synthesized by a Au-nanocluster catalyzed vapor-liquid-solid method.²⁹ The synthesis process is carried out in a horizontal quartz tube (inner diameter 45 mm, length 120 cm) mounted inside a single zone furnace. Inside the tube, CdS powders (Sigma-Aldrich Inc., 99.99% purity) are used as source and placed on an alumina boat in the center of the heating zone. Silicon (Si) wafers (QI Electronics Inc.) covered with 10-nm-thick Au film by sputtering are placed downstream from CdS powders near the end of the heating zone. A high purity nitrogen gas flow with a flow rate of 700 SCCM is introduced into the system to purge oxygen out. After 1-hour gas flow cleaning, the furnace is heated from room temperature to 850 °C in 20 minutes under 500 mbar pressure and kept at 850 °C for 1 hour afterwards. Meanwhile, a 155 SCCM nitrogen gas flow was maintained in the whole heating process to transport the evaporated CdS vapor to the Au-catalyzed Si substrates to initialize NW growth. The local temperature for Si substrate is about 650 °C. After 1 hour growth, yellowish NW products can be found on the Si substrate. For biological use, the NW-carried wafer is immersed into ethanol and sonicated in an ultrasonic cleaner for about 10 min to detach the NWs from the substrate. After removing the Si substrate and centrifuging the remaining solution, the NWs are separated from ethanol, then re-dispersed into phosphate buffered saline (PBS) solution, and finally sterilized under the UV lamp for about 1 hour in a laminar flow hood before culturing with the cells.

Previous work has shown that Si NWs either with^{7,30} or without surface modifications^{5,8} can be internalized by multiple cell lines at the single-cell level through an endogenous phagocytosis pathway. Here we select the human umbilical vascular endothelial cells (HUVEC) as a model cell line, since they serve as the inner layer of blood vessels and can be targeted in the future *in vivo* applications. The CdS NWs are internalized into the cells without any surface modification.

The HUVECs (Cat. No. C-015-5C) are cultured in Medium 200 (Cat. No. M-200-500) mixed with low serum growth supplement kit (Cat. No. S-003-K) in a mixing volume ratio of 50:1 (all purchased from Thermo Fisher Scientific, USA). HUVECs are grown on cell-culture-treated dishes which are suitable for cell attachment and incubated in a 37 °C, 5% CO₂/95% air, and humidified cell culture incubator. The NW-contained PBS solution is added into culture medium and incubated with cells for about 24 hours to ensure full internalization before measurement. NW lasing and sensing measurements inside cells are performed in an ambient environment using a home-made microscope system. For confocal microscopy, the cells are first fixed with 5% formaldehyde, and then stained with tetramethylrhodamine-phalloidin for cytoskeleton and Hoechst 33258 for nuclei. For scanning electron microscopy (SEM), the cells are further post-fixed with 1% osmium tetroxide in distilled water for 1 hour, dehydrated using 50%, 70%, 80%, 95%, and 100% ethanol each time for 10 minutes, and finally chemically dried using hexamethyldisilazane (HMDS). Prior to imaging, the cells are deposited with a thin Au/Pd film by sputtering. Since the NW is buried (sometimes deeply) under the cell surface, backscattered electron (BSE) in SEM is used to image the position and morphology (e.g., diameter) of NWs inside cells, while secondary electron (SE) analysis can only see the cell's surface and topography but not the buried NW. In BSE, NWs composed of heavy atoms (Cd, S) will backscatter electrons more strongly than cell cytoskeleton composed of light atoms (C and O, etc.), thus enabling a sharp imaging contrast.

To study the characteristics of the NW lasers inside living cells, we construct an inverted microscope system, as schematically illustrated in Fig. 1b. To excite the CdS NW, 479 nm laser pulses (5 ns pulse width, 20 Hz repetition rate) from an optical parametric oscillator are focused to a spot size of ~100 μm in diameter through a 50X objective lens. The 479 nm pumping intensity is adjusted through a continuously variable neutral density filter, generally controlled in the range of 0.1-20 μJ/mm². Higher intensity might ablate the NWs. The emitted light scattered from the NW end-facets is collected by the same objective, passed through a long-pass filter with 500 nm cut-off wavelength, and detected concurrently by a CCD camera for imaging and a spectrometer with a resolution of 0.02 nm (Horiba iHR550 with a 2400 g mm⁻¹ grating).

Results and discussion

The lasing mechanism of the NW can be described as follow. Due to its high RI ($n=2.67$), each NW end-facet serves as a reflective mirror, thus forming an analogous “Fabry-Perot” (F-P) cavity. Taking an NW of 200 nm in diameter and 3.5 μm in length as an example, the TE_{01} mode exhibits the largest reflectivity of about 24% among all three transverse modes (HE_{11} , TE_{01} , and TM_{01}) that are possibly supported by the NW, resulting in a quality factor, Q-factor, of ~ 50 .^{25,28} Although the Q-factor is relatively low, the NWs can provide a very high gain up to a few thousand per centimeter at a carrier density of $1\text{-}3 \times 10^{19} \text{ cm}^{-3}$,³¹ which is sufficient to compensate for the cavity loss to achieve lasing. Figure 2a shows an exemplary lasing spectrum of a 7 μm long (diameter ≈ 250 nm) NW in a living HUVEC, with the dominant lasing peak centered at 511.1 nm and the corresponding peak linewidth of 0.42 nm. Multimode lasing peaks resulting from different transverse modes can also be observed. A lasing threshold of about $1 \mu\text{J}/\text{mm}^2$ can be deduced from Fig. 2b, which is similar to that for the intracellular microsphere-based lasers^{14,15}, but one or two orders of magnitudes lower than that for the plasmon-based spasers¹³. Strong luminous spots can be seen at both end-facets of the NW (Fig. 2b inset) with clear interference rings that indicate the high coherence of the stimulated emission.

To confirm that the NW could be internalized into the HUVEC, both SEM (Fig. 2a inset) and confocal microscopy (Fig. 2c) are performed for the same NW. For confocal microscopy, the cell cytoskeleton is stained red and the nuclei is stained blue. The CdS NW can be visualized by its own green fluorescence under 488 nm laser excitation. A typical z-stack confocal microscopy image is shown in Fig. 2c, with cell nuclei (blue), cytoskeleton (red) and NW (green) clearly resolved. The cross-sections along (right in Fig. 2c) and perpendicular (bottom in Fig. 2c) to the NW axis are also reconstructed, which unambiguously verify that the NW is fully internalized by HUVECs. A much shorter CdS NW ($D \approx 190$ nm, $L = 3.5 \mu\text{m}$) is also investigated (Fig. 2d-f), with a blue-shifted lasing wavelength of 500.5 nm, wider peak linewidth of 0.56 nm (Fig. 2d), and a slightly higher lasing threshold ($2.3 \mu\text{J}/\text{mm}^2$, Fig. 2e).

We then use this 3.5 μm long NW to demonstrate intracellular micro-environment sensing. With sodium chloride (NaCl) solution added to the cell culture medium, the HUVECs first shrink in response to the hypertonic stress with a net efflux of intracellular water out of cells, and then partially recover through a Na^+/H^+ exchange-mediated regulatory volume increase. In this process, the cell volume change causes intracellular solute concentration to vary, which in turn results in an RI change of the cell cytoplasm. By detecting the NW lasing wavelength that is

dependent on the surrounding RI, we can monitor cell environment changes in real time. Fig. 3 shows the lasing spectrum measurement carried out every 40 seconds, including a 20-second spectrum integration time followed by a 20-second interval time. At the very beginning, we perform a blank test to investigate the situation without NaCl addition, as shown in Figure 3a, $t=0-700$ s. It can be seen that the lasing peak wavelength of the NW in the cell remains nearly unchanged at 504.1 nm with only a slight deviation of about 0.1 nm, suggesting that without NaCl addition, the cellular environment changes by the cell itself have a negligible effect on the lasing wavelength. Then an additional 2 g/L (final concentration value after mixing) NaCl is added into the cell culture medium, which initially contains 8 g/L NaCl (the moment when the NaCl solution is added is marked by the first black arrow in Fig. 3a). This NaCl addition process is conducted for three more times later on to verify its repeatability (Fig. 3a). It can be seen that each time when the NaCl is added, a red-shift in the lasing wavelength occurs nearly instantly (within 40 seconds), followed by a relatively slow blue-shift to the baseline, which is quite consistent with the expected shrinkage and recovery process described above. A maximum red-shift of 0.55 nm can be observed in the first NaCl addition cycle ($t=750-1500$ s in Fig. 3a), with the corresponding lasing spectral evolution shown in Fig. 3b. In contrast to the organic dyes, the NW lasing does not suffer a photobleaching issue. The lasing emission persists for hours without observable intensity reduction.

The NW laser sensitivity for NaCl-induced cell volume change is analyzed as follow. Based on the Boyle-van't Hoff law (which states the product of osmolality and equilibrium volume of the osmotically active portion of the cell is constant), the shrunk cell volume V (with non-water fraction of cell volume deducted) after NaCl addition can be roughly estimated by^{14,32}

$$V = \frac{\Pi_0}{\Pi} V_0 = 0.81V_0, \quad (1)$$

where V_0 , Π_0 , and Π are the initial cell volume (with non-water fraction deducted), the initial (298 mOsm/L) and final osmotic concentration (366 mOsm/L), respectively. The RI change from the initial RI $n_0=1.37$ to final RI n is given by³³

$$\frac{n_0 - n_w}{n - n_w} = \frac{c_0}{c} = \frac{V}{V_0}, \quad (2)$$

where n_w , c_0 , and c are the RI of water and initial and final cell solutes concentration. Based on Eqs. 1-2, the RI change of $(n - n_0)=0.01$ due to the cell volume shrinkage can be obtained

and a sensitivity of about 55 nm/RIU can be deduced for the NW laser. Given the lasing peak linewidth of 0.56 nm and the standard deviation of about 0.1 nm of the lasing peak, an FOM of 98 and a detection limit of 1.8×10^{-3} RIU can be achieved. Eventually, the lasing baseline gradually increases after each NaCl addition, which may attribute to the reduced ability of the cell to recover from the shrinkage.

On the other side, the NW sensitivity can be only determined by its geometry. Theoretically, the lasing wavelength can be considered to be equal to the resonance wavelength λ of the NW F-P cavity, which can be written as²⁵

$$\lambda = 2n_{eff}L/m, \quad (3)$$

where n_{eff} is the effective RI of the NW (i.e., the propagation constant of the NW waveguide), L is the NW length, m is an integer denoting the longitudinal mode order. Differentiating both sides of Eq. (3), the sensitivity of the NW can be deduced as

$$\frac{d\lambda}{dn} = \frac{dn_{eff}}{dn} * \frac{\lambda}{n_{eff}}. \quad (4)$$

We can see that the sensitivity is particularly affected by n_{eff} , which in turn depends on the NW parameters along the cross-section (e.g., diameter and NW RI distribution), but is independent of the NW length. In Fig. 4a, we use Comsol simulation to calculate n_{eff} for the three lowest-order transverse modes (HE_{11} , TE_{01} , and TM_{01}) for the NW with a diameter range of 180-240 nm and obtain the corresponding sensitivity through Eq. (4). To decide which mode contributes to lasing and sensing, lasing thresholds of HE_{11} , TE_{01} , and TM_{01} mode for NWs with a fixed length of 3.5 μm (the length of the NW used in Fig.3a) is analyzed by finite-difference time-domain (FDTD) software.²⁸ Fig. 4b shows the gain needed to achieve lasing for those three modes. The diameter of the NW inside the cell is confirmed by SEM (Fig. 2d inset) with an estimated value of approximately 190 nm. It is apparent that for the 190-nm-diameter NWs the TE_{01} mode exhibits the lowest lasing threshold (threshold gain = 5400 cm^{-1}). Based on these pieces of evidence, we conclude that it is the TE_{01} mode that is responsible for the lasing peak observed in Fig. 3. It is seen from Fig.4a that when the diameter is about 190 nm, the sensitivity of TE_{01} mode of 52 nm/RIU shows good agreement with our experimental results, which proves that the wavelength shift is indeed caused by the NaCl-induced cell volume changes. The electrical field distribution for the TE_{01} mode of a 190-nm-diameter NW at 504 nm wavelength is shown in Fig. 4c with ~18%

electric field energy outside NW, facilitating a sensitive detection of the cellular environmental changes.

Finally, to examine the cytotoxicity of the bare CdS NWs to HUVECs, we test the viability of the NW-treated cells over the course of one week by using calcein AM and ethidium homodimer as live/dead indicators. Live cells exhibit bright green fluorescence, whereas dead cells with compromised membranes show red fluorescence (see Fig. S1). The same amount of NW-containing solution is added into multiple petridishes at the same time in the beginning of observation period. Each day, we randomly select ten areas ($166\ \mu\text{m} \times 123\ \mu\text{m}$) of cells on one petridish for viability test. In each area, there are 10-30 NWs. Fig. 5 shows typical brightfield and green-fluorescence microscope images of the NW-treated cells. It can be seen that even after 7-day NW culturing, these cells stay alive and healthy with nearly 100% viability. Over this period, the cells rapidly proliferate from a density of $2.5 \times 10^3\ \text{cells}/\text{cm}^2$ to $1\sim 4 \times 10^5\ \text{cells}/\text{cm}^2$, which indicates successful cell division. On the 5th day, one batch of the NW-treated cells are dislodged from the original petridish and subcultured into new dishes with diluted seeding density. 24 hours after subculturing, these cells are tested again (see Fig. S2), showing viability and good proliferation capability. The subcellular distribution of NWs is also investigated (see Figs. S3 and S4). We find that NWs are distributed within the cytoplasmic compartment of HUVECs without entering the nucleus, which is understandable since the nuclear pores have a diameter of only about $5\ \text{nm}$ ³⁴.

Conclusions

In summary, we have demonstrated stand-alone intracellular laser probes based on semiconductor NWs with $<0.5\ \mu\text{m}^3$, which can potentially reduce the perturbations to the cells and increase the number of probes inside the cell. Owing to the strong evanescent field presence near the NW surface and the narrow lasing emission linewidth, the laser probes show a sensitivity of about $55\ \text{nm}/\text{RIU}$ and an FOM of approximately 98 to detect the intracellular environment changes. Future work may include the achievement of the lasing from the higher order modes (such as TM_{01} , see Fig. 4a) that have a higher RI sensitivity. Surface modification methods can be introduced to facilitate spontaneous internalization of NW probes into different cell types, such as ovary⁵ and neuron⁸ cells. Overall, our NW laser probes may enable continuous

monitoring of intracellular activities and biochemical signals with high spatial and temporal resolution in various biological and biomedical applications.

Acknowledgements

The authors acknowledge the support from the National Science Foundation (ECCS-1607250) and the International Postdoctoral Exchange Fellowship Program (No. 20160007). The authors wish to thank Kai Sun, Hongbo Zhu, and Xiaotian Tan for helpful discussions.

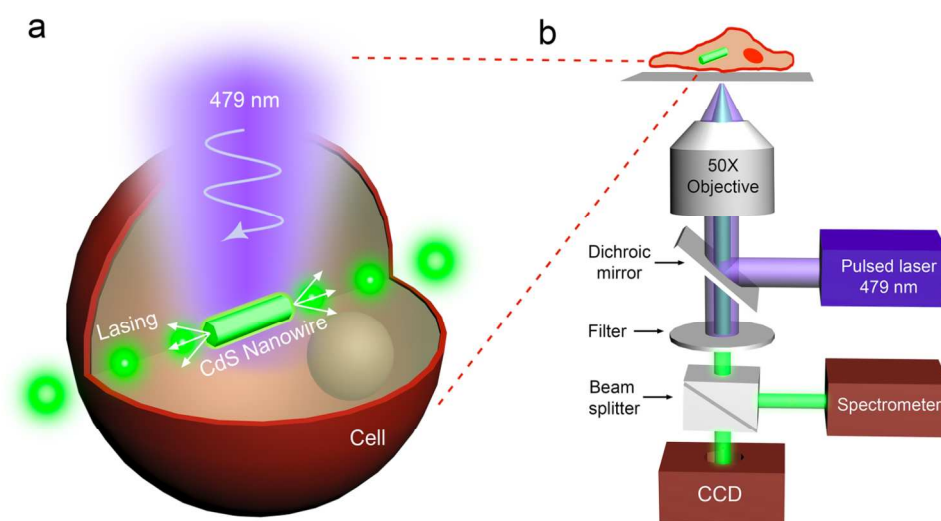


Figure 1. (a) Illustration of a CdS NW laser inside a cell. (b) Schematic diagram of experimental setup for optical characterization of the intracellular NW laser.

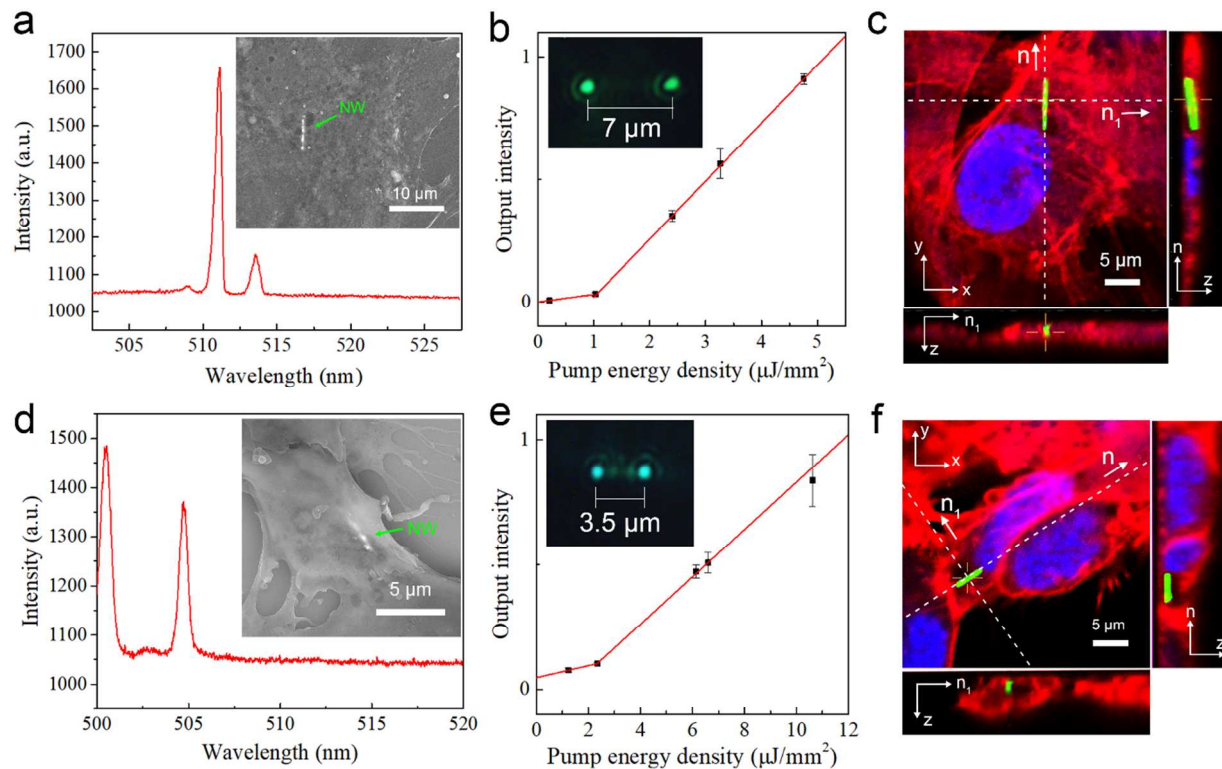


Figure 2. (a) Lasing spectrum, (b) threshold curve, (c) confocal image of a 7 μm long NW inside an HUVEC. (d) Lasing spectrum, (e) threshold curve, (f) confocal image of a 3.5 μm long NW inside another HUVEC. Inset of (a) and (d): SEM image of the NW inside the cell. Inset of (b) and (e), dark-field CCD images of the lasing emission from the corresponding NWs. Right and bottom panel in (c) and (f): z-section images along the white dashed line n (parallel to the NW axis) and n_1 (perpendicular to the NW axis), respectively.

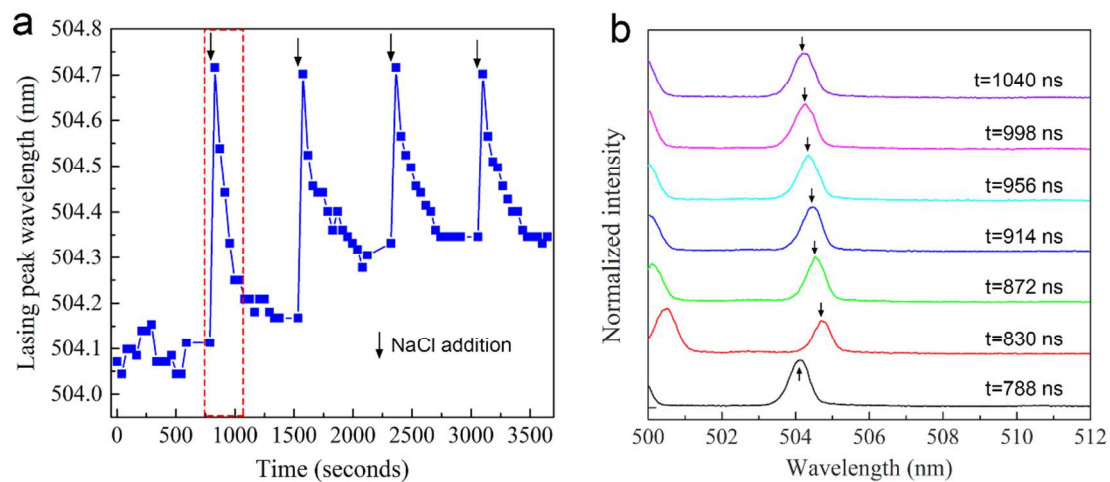


Figure 3. (a) Temporal measurement of a lasing peak wavelength from a 3.5 μm long NW ($D \approx 200$ nm) inside an HUVEC. The black arrows indicate the moments when an additional 2 g/L NaCl is added into the cell culture medium. (b) Lasing spectra evolution of the NW laser probe in one NaCl-addition cycle (marked by red box in (a)). Curves are vertically shifted for clarity. Arrows indicate the lasing peak wavelength.

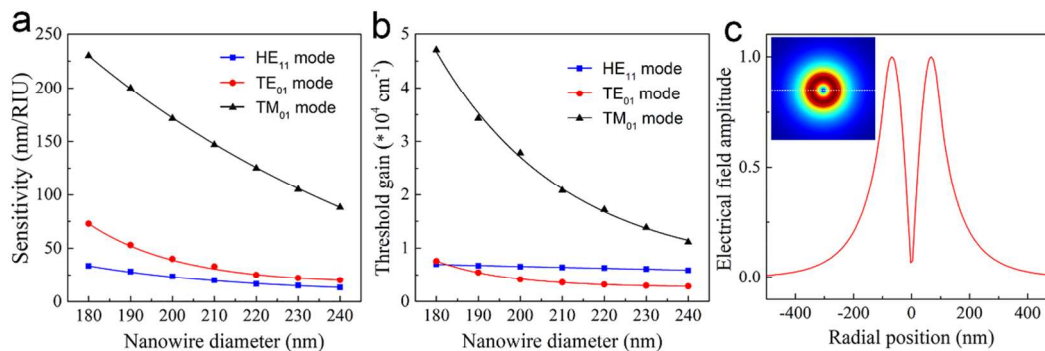


Figure 4. (a) Calculated refractive index sensitivity of HE₁₁, TE₀₁, and TM₀₁ mode for different NW diameters at the lasing wavelength of 504.1-nm. (b) Calculated lasing threshold gain for HE₁₁, TE₀₁, and TM₀₁ mode of a 3.5 μm long NW as a function of the NW diameter. (c) Electrical field amplitude of a CdS NW of 190 nm in diameter along the radial direction (the dashed line in inset). Inset: electrical field amplitude distribution.

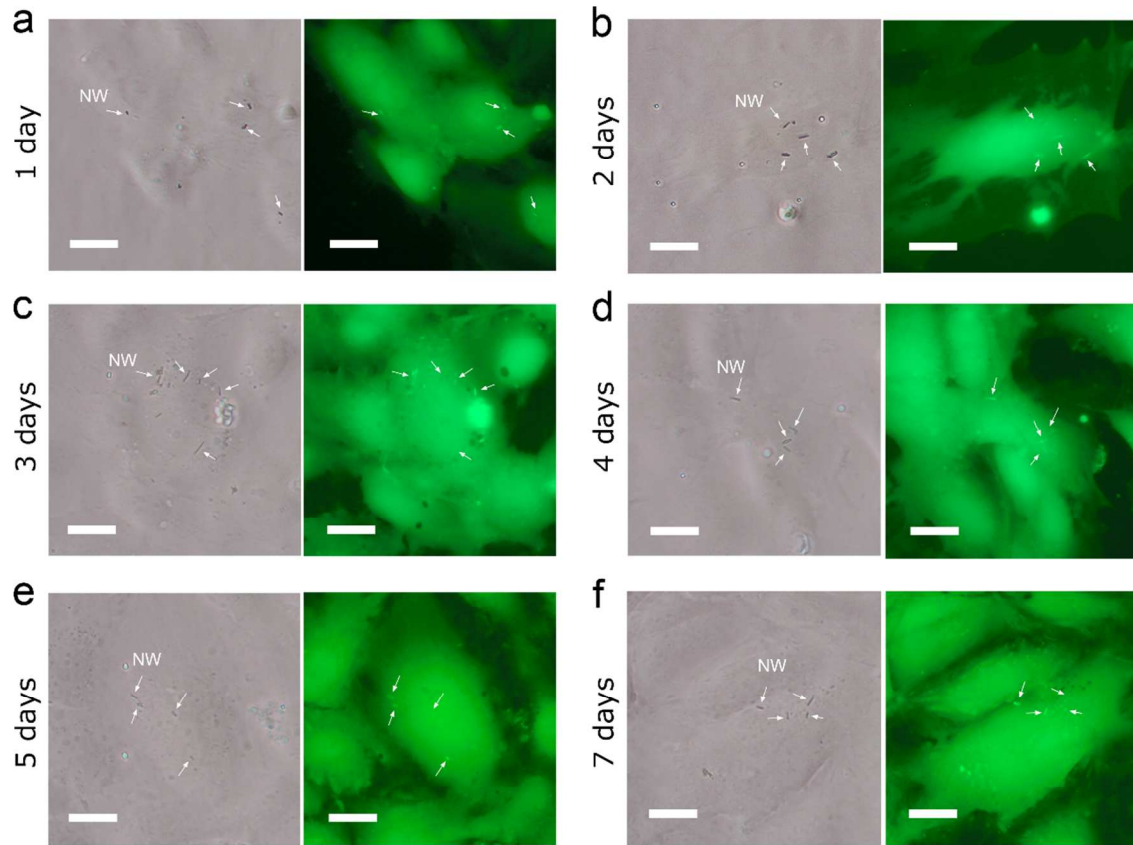
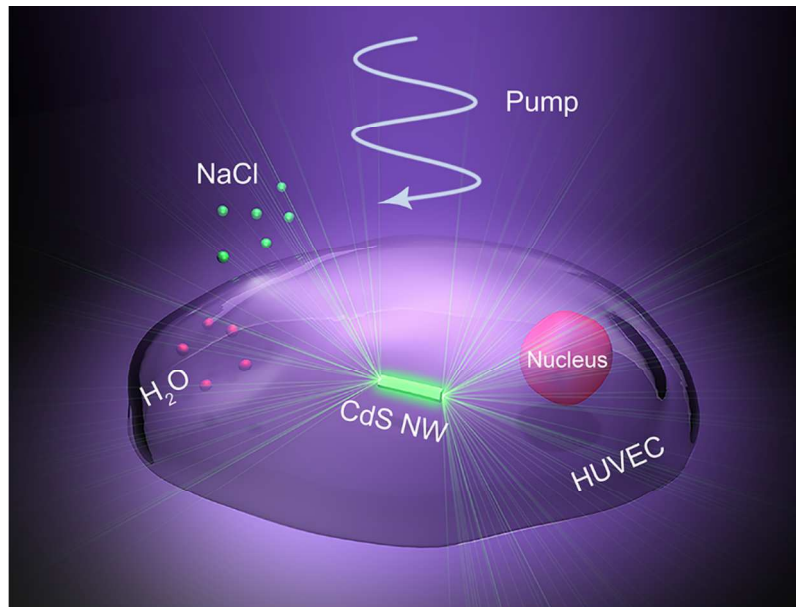


Figure 5. Live/dead cell assay for cytotoxicity analysis. Brightfield and green-fluorescence microscope images of the HUVECs incubated with CdS NWs for 1 day (a), 2 days (b), 3 days (c), 4 days (d), 5 days, (e) and 7 days (f), respectively. The cells under test are stained with 0.4 μM calcein AM and 0.4 μM ethidium homodimer. Healthy cells exhibit green fluorescence (calcein AM), whereas dead cells exhibit red fluorescence (ethidium homodimer). Note that red-fluorescence images are not shown here. They are all dark, as no cells are dead. The white arrows point the position of NWs (shown as dark or black lines in the brightfield images). In the corresponding green-fluorescence images, some of the NWs can be seen as green lines with brighter green color than the background since the NWs can also emit green fluorescence. Some of the NWs cannot be seen in the corresponding positions, probably because these NWs are submerged deeply in the cell plasma and their fluorescence are embedded in the green background. Scale bars, 10 μm .

References:

- ¹ I. Hafez, K. Kisler, K. Berberian, G. Dernick, V. Valero, M. G. Yong, H. G. Craighead, and M. Lindau, Electrochemical imaging of fusion pore openings by electrochemical detector arrays, *Proc. Natl. Acad. Sci. U. S. A.*, 2005, **102**, 13879-13884.
- ² C. Xie, Z. Lin, L. Hanson, Y. Cui, and B. Cui, Intracellular recording of action potentials by nanopillar electroporation, *Nat. Nanotechnol.*, 2012, **7**, 185-190.
- ³ M. E. Spira and A. Hai, Multi-electrode array technologies for neuroscience and cardiology, *Nat. Nanotechnol.*, 2013, **8**, 83-94.
- ⁴ R. Yan, J. H. Park, Y. Choi, C. J. Heo, S. M. Yang, L. P. Lee, and P. Yang, Nanowire-based single-cell endoscopy, *Nat. Nanotechnol.*, 2011, **7**, 191-196.
- ⁵ W. Zhang, L. Tong, and C. Yang, Cellular binding and internalization of functionalized silicon nanowires, *Nano Lett.*, 2012, **12**, 1002-1006.
- ⁶ G. Shambat, S. R. Kothapalli, J. Provine, T. Sarmiento, J. Harris, S. S. Gambhir, and J. Vuckovic, Single-cell photonic nanocavity probes, *Nano Lett.*, 2013, **13**, 4999-5005.
- ⁷ J. F. Zimmerman, G. F. Murray, Y. Wang, J. M. Jumper, J. R. Austin, 2nd, and B. Tian, Free-Standing Kinked Silicon Nanowires for Probing Inter- and Intracellular Force Dynamics, *Nano Lett.*, 2015, **15**, 5492-5498.
- ⁸ J. H. Lee, A. Zhang, S. S. You, and C. M. Lieber, Spontaneous Internalization of Cell Penetrating Peptide-Modified Nanowires into Primary Neurons, *Nano Lett.*, 2016, **16**, 1509-1513.
- ⁹ A. Zhang and C. M. Lieber, Nano-Bioelectronics, *Chem. Rev.*, 2016, **116**, 215-257.
- ¹⁰ U. Resch-Genger, M. Grabolle, S. Cavaliere-Jaricot, R. Nitschke, and T. Nann, Quantum dots versus organic dyes as fluorescent labels, *Nat. Methods*, 2008, **5**, 763-775.
- ¹¹ S. W. Bae, W. Tan, and J. I. Hong, Fluorescent dye-doped silica nanoparticles: new tools for bioapplications, *Chem. Commun.*, 2012, **48**, 2270-2282.
- ¹² J.-M. Liu, J.-T. Chen, and X.-P. Yan, Near infrared fluorescent trypsin stabilized gold nanoclusters as surface plasmon enhanced energy transfer biosensor and in vivo cancer imaging bioprobe, *Anal. Chem.*, 2013, **85**, 3238-3245.
- ¹³ E. I. Galanzha, R. Weingold, D. A. Nedosekin, M. Sarimollaoglu, J. Nolan, W. Harrington, A. S. Kuchyanov, R. G. Parkhomenko, F. Watanabe, Z. Nima, A. S. Biris, A. I. Plekhanov, M. I. Stockman, and V. P. Zharov, Spaser as a biological probe, *Nat. Commun.*, 2017, **8**, 15528.
- ¹⁴ M. Humar and S. H. Yun, Intracellular microlasers, *Nat. Photonics*, 2015, **9**, 572-576.
- ¹⁵ M. Schubert, A. Steude, P. Liehm, N. M. Kronenberg, M. Karl, E. C. Campbell, S. J. Powis, and M. C. Gather, Lasing within Live Cells Containing Intracellular Optical Microresonators for Barcode-Type Cell Tagging and Tracking, *Nano Lett.*, 2015, **15**, 5647-5652.
- ¹⁶ M. Humar, A. Upadhyaya, and S. H. Yun, Spectral reading of optical resonance-encoded cells in microfluidics, *Lab Chip*, 2017, **17**, 2777-2784.
- ¹⁷ M. Humar, A. Dobravec, X. Zhao, and S. H. Yun, Biomaterial microlasers implantable in the cornea, skin, and blood, *Optica*, 2017, **4**, 1080-1085.
- ¹⁸ N. W. Kam, M. O'Connell, J. A. Wisdom, and H. Dai, Carbon nanotubes as multifunctional biological transporters and near-infrared agents for selective cancer cell destruction, *Proc.*

- Natl. Acad. Sci. U. S. A.*, 2005, **102**, 11600-11605.
- ¹⁹ X. Chen, A. Kis, A. Zettl, and C. R. Bertozzi, A cell nanoinjector based on carbon nanotubes, *Proc. Natl. Acad. Sci. U. S. A.*, 2007, **104**, 8218-8222.
- ²⁰ S. Kruss, A. J. Hilmer, J. Zhang, N. F. Reuel, B. Mu, and M. S. Strano, Carbon nanotubes as optical biomedical sensors, *Adv. Drug. Deliv. Rev.*, 2013, **65**, 1933-1950.
- ²¹ S. Kruss, D. P. Salem, L. Vukovic, B. Lima, E. Vander Ende, E. S. Boyden, and M. S. Strano, High-resolution imaging of cellular dopamine efflux using a fluorescent nanosensor array, *Proc. Natl. Acad. Sci. U. S. A.*, 2017, **114**, 1789-1794.
- ²² S. Cho, M. Humar, N. Martino, and S. H. Yun, Laser Particle Stimulated Emission Microscopy, *Phys. Rev. Lett.*, 2016, **117**, 193902.
- ²³ X. Fan and S. H. Yun, The potential of optofluidic biolasers, *Nat. Methods*, 2014, **11**, 141-147.
- ²⁴ R. Matthes, C. Cain, D. Courant, D. Freund, B. Grossman, P. Kennedy, D. Lund, M. Mainster, A. Manenkov, and W. Marshall, Revision of guidelines on limits of exposure to laser radiation of wavelengths between 400 nm and 1.4 μ m, *Health Phys.*, 2000, **79**, 431-440.
- ²⁵ M. A. Zimmler, F. Capasso, S. Müller, and C. Ronning, Optically pumped nanowire lasers: invited review, *Semicond. Sci. Tech.*, 2010, **25**, 024001.
- ²⁶ Y. G. Ma, X. Guo, X. Q. Wu, L. Dai, and L. M. Tong, Semiconductor nanowire lasers, *Adv. Opt. Photon.*, 2013, **5**, 216-273.
- ²⁷ S. W. Eaton, A. Fu, A. B. Wong, C.-Z. Ning, and P. Yang, Semiconductor nanowire lasers, *Nat. Rev. Mater.*, 2016, **1**, 16028.
- ²⁸ X. Q. Wu, Q. Chen, P. Z. Xu, L. M. Tong, and X. Fan, Refractive index sensing based on semiconductor nanowire lasers, *Appl. Phys. Lett.*, 2017, **111**, 031112.
- ²⁹ C. Ma and Z. L. Wang, Road map for the controlled synthesis of CdSe nanowires, nanobelts, and nanosaws—a step towards nanomanufacturing, *Adv. Mater.*, 2005, **17**, 2635-2639.
- ³⁰ J. F. Zimmerman, R. Parameswaran, G. Murray, Y. Wang, M. Burke, and B. Tian, Cellular uptake and dynamics of unlabeled freestanding silicon nanowires, *Sci. Adv.*, 2016, **2**, e1601039.
- ³¹ A. Maslov and C. Ning, Modal gain in a semiconductor nanowire laser with anisotropic bandstructure, *IEEE J. Quantum Elect.*, 2004, **40**, 1389-1397.
- ³² R. C. Prickett, J. A. Elliott, S. Hakda, and L. E. McGann, A non-ideal replacement for the Boyle van't Hoff equation, *Cryobiology*, 2008, **57**, 130-136.
- ³³ C.-Y. Tan and Y.-X. Huang, Dependence of Refractive Index on Concentration and Temperature in Electrolyte Solution, Polar Solution, Nonpolar Solution, and Protein Solution, *J. Chem. Eng. Data*, 2015, **60**, 2827-2833.
- ³⁴ D. Mohr, S. Frey, T. Fischer, T. Guttler, and D. Gorlich, Characterisation of the passive permeability barrier of nuclear pore complexes, *Embo Journal*, 2009, **28**, 2541-2553.



A nanowire laser as an intracellular probe.